Journal of Materials Chemistry A

PAPER

View Article Online
View Journal | View Issue

Cite this: J. Mater. Chem. A, 2015, 3, 12761

Fibrous and flexible supercapacitors comprising hierarchical nanostructures with carbon spheres and graphene oxide nanosheets

Xiong Zhang,†[a] Yuekun Lai,†[ab] Mingzheng Ge,[a] Yaxin Zheng,[c] Ke-Qin Zhang*[ab] and Zhiqun Lin*[d]

Received 4th May 2015
Accepted 7th May 2015

DOI: 10.1039/c5ta03252k

www.rsc.org/MaterialsA

A fibrous, flexible supercapacitor (FFSC) electrode with unique layer-by-layer structures is constructed using a one-step electrophoretic method. The highly enhanced capacitance of 53.56 mF cm^{-2} and good charge/discharge stability is attributed to the synergistic effect between the GO nano-sheet and carbon nano-sphere for electrolyte contact and ion transportation. Such a construction method can be employed to construct various FFSC electrodes for portable energy storage and wearable electronics applications.

Introduction

In response to the changing global landscape, energy has become a primary focus for major corporations and scientific communities all over the world. There has been increasing interest in developing and refining efficient energy storage devices. The task of developing sustainable and renewable energy has been one of the most important focuses of this movement.[1–5] Among the various energy storage systems, supercapacitors, also known as ultracapacitors, have matured significantly over the last decade. These powerful devices have recently emerged with potential to facilitate major advances in energy storage. Supercapacitors exhibit exceptional properties, including high power density, fast rates of charge/discharge, reliable cycling life, and safe operation,[6,7] making them advantageous for efficient electrical energy storage.[8] Carbon-based materials with good electrical conductivity, higher surface area, lower cost, and more established fabrication techniques are usually adopted as electrode materials for EDLCs.[9,10] Conducting polymers and metal oxides are usually employed as electrode materials for pseudocapacitors or redox supercapacitors.[11,12] It is interesting to note that supercapacitors have been especially promising in the fields of portable and highly integrated equipment such as electronic textiles and wearable electronics that require small, lightweight and high flexible devices. Unlike film-structured devices, the fibrous devices can be readily embedded into the textile at ideal locations, while retaining the fabric's mechanical flexibility. Investigation into fibrous devices has provided intriguing prospects for the scientific community, however, many challenges still remain.[13]

Graphene, a novel carbonous material with a two-dimensional (2D) nanostructure, has attracted much attention in both fundamental science and applied research.[14,15] It has been widely recognized as a promising electrode material for supercapacitors as it carries many superior properties,[16–21] including exceptional thermal stability, optimal mechanical stiffness, excellent electronic properties and electrical conductivity, high surface area (theoretically over 2630 m^2 g^{-1} per single layer), and flexibility, for many potential applications in electronics and transistors.[22–27] Graphene-based film materials are promising candidates for flexible and micro-energy storage devices.[28–33] To prevent the agglomeration of graphene sheets, much effort has been devoted to mixing graphene with polymers or inorganic nanoparticles to yield graphene-incorporated composites.[34,35] Recently, significant progress has been made towards the development of highly flexible and wire-shaped devices to realize energy harvesting and storage for flexible and wearable electronics,[36–40] for example, a sandwich-like supercapacitor electrode with carbon-based composites was developed and exhibited an outstanding capacitor performance.[41–43] Notably, some studies have been conducted to construct fibrous and flexible supercapacitor (FFSC) devices by taking advantage of the synergistic effect of multiple active materials, such as pen ink and polyaniline composite fibers.[37,38]

Herein, we report on the crafting of a unique hierarchical nanostructure composed of graphene nanosheets and carbon nanospheres *via* a simple one-step electrophoretic deposition method. Carbon nanospheres acting as nanospacers were

[a]National Engineering Laboratory for Modern Silk, College of Textile and Clothing Engineering, Soochow University, Suzhou, Jiangsu 215123, China. E-mail: kqzhang@suda.edu.cn

[b]Research Center of Cooperative Innovation for Functional Organic, Polymer Material Micro, Nanofabrication, Soochow University, Suzhou, Jiangsu 215123, China

[c]Department of Electrical and Computer Engineering, University of Waterloo, Ontario, N2L 3G1, Canada

[d]School of Materials Science and Engineering, Georgia Institute of Technology, Atlanta, Georgia 30332, USA. E-mail: zhiqun.lin@mse.gatech.edu

† These authors contributed equally.

introduced into graphene nanosheets to render the formation of ideal layer-by-layer hierarchical nanostructures. Subsequently, this unique GO nanosheet and carbon nanosphere hierarchical nanostructure (GCHN) composite was exploited as the building block to produce supercapacitor electrodes and fibrous and flexible supercapacitors (FFSCs). As nanospacers, carbon spheres not only provided rapid diffusion velocity between the electrolyte and the surface of the electrode, but also increased the utilization efficiency of graphene. Electrochemical performance on specific capacitance and reversible capacity has been systematically studied. The synergistic effects of the capacitance behavior of the fibrous and flexible GCHN electrode, and the device with unique layer-by-layer hierarchical nanostructures on capacitance were also scrutinized as a function of deposition time and GO content. The long-term cycle stability of the fibrous and flexible supercapacitor (FFSC) was also evaluated.

Experimental section

Synthesis of carbon spheres

Carbon nanospheres are freshly prepared by hydrothermal treatment of glucose according to previous reports.[44–46] Specifically, glucose (4–8 g) was dissolved in deionized (DI) water (40 mL) to form a clear solution. The mixture was transferred to a Teflon-sealed autoclave and oven-dried at 180 °C for more than 4 h. The resulting black or puce products were isolated and cleaned by three cycles of centrifugation, washing, and dispersion in DI water and alcohol. Finally, the compound was dried in an oven at 80 °C for a minimum of 1 h to obtain dark brown solid spherical pellets for the subsequent experiments. The spheres were kept dry and stored at room temperature.

Preparation of graphene oxide

Graphene oxide (GO) was synthesized using a modified Hummer's method.[47] In a typical synthesis process, 1.0 g of raw graphite powder (SP-1, Bay Carbon) with 0.5 g of $K_2S_2O_8$ (Fluka) and 0.5 g of P_2O_5 (Fluka) was stirred in 1.5 mL of H_2SO_4 solution at 80 °C for 4.5 h; pre-oxidized graphite was obtained after subsequent filtration with DI water for at least 3 times. After drying in air overnight, the preoxidized graphite powder was further oxidized in 23 mL of H_2SO_4 solution with gradual addition of 3 g of $KMnO_4$ (Sigma-Aldrich) at 0 °C. After stirring the solution at 36 °C for 2 h, 46 mL of DI water was added and stirred for 2 h. The oxidation ended with adding 140 mL of DI water and 2.5 mL of H_2O_2 (35%) when the solution colour changed to light brown. The GO solution was washed, filtered with 10% HCl, then redispersed in DI water that had been dialyzed for 2 weeks.

Fabrication of the FFSC electrode

The as-prepared carbon spheres (0.5 mg) and DI water (10 mL) were successively added into 10 mL ethanol and sonicated for 10 min at room temperature. Then, a certain volume of the above-mentioned carbon sphere solution (0.25 mg mL^{-1}) was added into 5 mL of 0.5 mg mL^{-1} GO nanosheet ethanol solution to obtain mixed solutions containing various mass ratios of the graphene/carbon spheres. A conductive fiber (a platinum wire was used in this work) was submerged into the mixed GO and carbon sphere solution in a stainless steel ring (height of approximately 12 mm) with plastic bottom; it was used as the anode during electrophoretic deposition. After the conductive fiber submerged into the solution, the DC power was turned on. The stainless steel ring acted as the cathode to establish a cylindrical electric field for depositing the GO and carbon spheres to yield a layer-by-layer structure. After the experiment time was reached, the fiber was taken out, and then the DC power was turned off. GO was chemically reduced through the immersion into hydroiodic acid (HI) solution at 100 °C for 1.5–2.0 h. The reduced graphene oxide (rGO) FFSC electrode was obtained after washing with DI water.[48]

Construction of the flexible supercapacitor device

Unlike conventional supercapacitors, which consist of two planar electrodes and a planar spacer to form a two-dimensional (2-D) planar structure, the flexible supercapacitor constructed here is enclosed in a metal or plastic shell filled with electrolyte. Briefly, we used a special encapsulating technique to assemble the FFSC supercapacitor device, which included two GCHN fiber electrodes with optimal 50.0 wt% GO content (weight ratio of GO/GO + carbon spheres), a cotton thread spacer wire, and an electrolyte. The cotton thread was evenly reeled over one GCHN FFSC electrode with a specific pitch to prevent short circuits caused by the direct contact of electrodes. The other GCHN FFSC electrode was then placed in parallel closely to the first electrode and packaged into a flexible plastic tube. Finally, the plastic tube was filled with electrolyte and sealed to construct the final supercapacitor device.

Characterization and electrochemical measurements

Optical photographs were taken by using a Nikon 4500 digital camera. The microscopic morphology of samples was characterized by field emission scanning electron microscopy (FESEM, S-4800, Hitachi) operating at 3.0 kV. The surface morphology of the GO sheets was investigated by using an atomic force microscope (AFM, MultiMode8, Bruker) in the tapping mode. The electrochemical performance of GCHN electrodes and the corresponding optimal FFSC devices (50.0 wt% of the GO content) was tested in 6 M KOH electrolyte by cyclic voltammetry (CV), galvanostatic charge/discharge (GCD), and electrochemical impedance spectroscopy (EIS) with a CHI 760D electrochemical workstation (Shanghai, China). The electrode experiments were carried out in a three-electrode system. The as-prepared GCHN FFSC electrode served as the working electrode; a platinum wire and a saturated calomel electrode (SCE) were used as counter and reference electrodes, respectively.

Results and discussion

Fig. 1A shows the SEM image of carbon nanospheres. Clearly, carbon nanospheres were uniform with an average diameter of 200 nm. The AFM image showed that the lateral dimension of

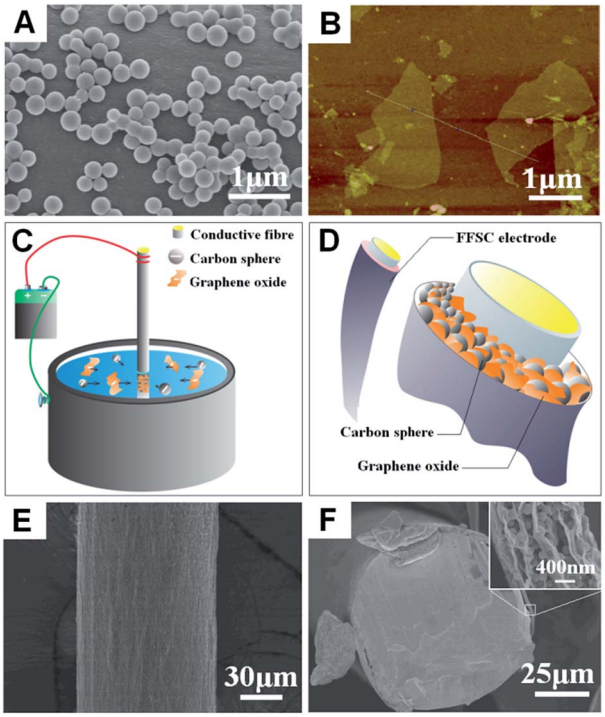

Fig. 1 (A) SEM image of carbon nanospheres. (B) AFM image of GO nanosheets on silicon. (C) Schematic illustration of the hierarchically nanostructured fibrous and flexible supercapacitor (FFSC) electrode comprising GO nanosheets and carbon spheres *via* an electrophoretic deposition approach. (D) The FFSC electrode based on hierarchical composite containing GO nanosheets and carbon nanospheres, with a unique self-assembled layer-by-layer structure. SEM image of the as-prepared FFSC electrode: (E) side-view, and (F) cross-sectional view. The inset of (F) is the zoom-in SEM image of the edge section of the as-constructed porous carbon sphere/GO structure.

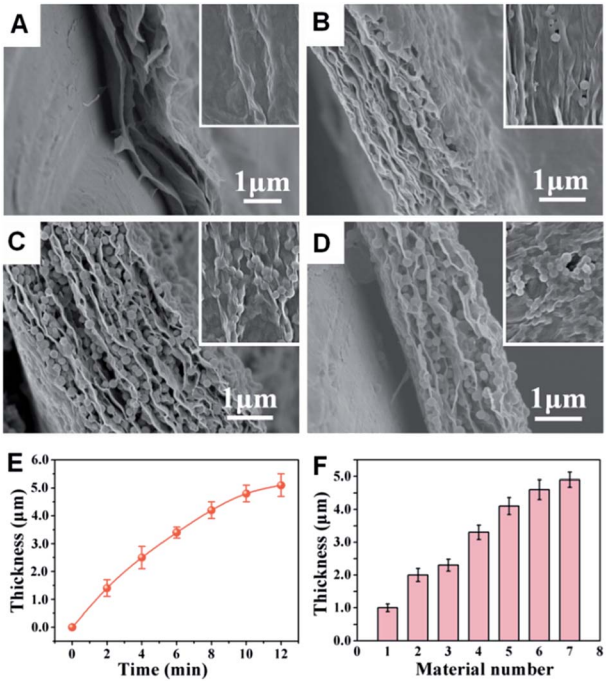

Fig. 2 (A) SEM image of the pristine GO nanosheet film with a deposition duration of 10 min (cross-sectional view). SEM images of the GCHN with (B) 66.7 wt% and (C) 50.0 wt% of GO content, respectively, with a 10 min deposition. (D) SEM image of the GCHN containing 50.0 wt% GO with 5 min deposition. (E) The relationship between the GCHN thickness and the deposition time. (F) Thickness of the GCHN with varied GO content after a 10 min deposition. From no. 1 to no. 8, the GO content is 100.0 wt%, 83.3 wt%, 80.0 wt%, 75.0 wt%, 66.7 wt%, 50.0 wt%, and 33.3 wt% respectively.

GO sheets was in the range of 0.2–2.0 μm (Fig. 1B). In neutral aqueous solution, carbon nanospheres and GO nanosheets had negative ζ-potentials of approximately −40.5 mV and −59.8 mV, respectively. Due to their similar negative charge potentials, carbon nanospheres and GO nanosheets were uniformly dispersed in solution and simultaneously deposited on the anode under a well-distributed circular electric field. This process occurred in the mixed solution of carbon nanospheres, GO, deionization water (DI water), and ethanol, accompanied by a redox reaction under DC at 10 V, shown in Fig. 1C. As the surface area of 2D GO nanosheets was much larger than that of carbon spheres, carbon nanospheres were dispersed between the GO nanosheets resulting in the layer-by-layer GCHN that wrapped tightly onto the surface of the wire electrode, as shown in Fig. 1D–F. The structure of the GCHN was dictated by the weight ratio of the GO content. With the addition of carbon nanospheres, the effective surface area of hierarchical nanostructure comprising carbon nanospheres and graphene nanosheets increased due to the fact that carbon spheres acted as nanospacers for separating the GO nanosheets, which is vital for improved electrochemical capacitance performance.

Fig. 2A shows the cross-sectional SEM image of the as-deposited pristine GO nanosheets film, without the addition of carbon spheres. Obviously, a very dense structure with extensive aggregation and close stacking of GO nanosheets is evident, suggesting that GO nanosheets tend to restack during the process of electrophoretic deposition. Fig. 2B–D compare the cross-sectional images of hierarchical nanostructures composed of carbon nanospheres and GO nanosheets formed in solution with different weight ratios of GO to carbon spheres (Fig. 2B and C) obtained from different deposition durations (Fig. 2C and D). It is interesting to note that a larger amount of carbon spheres was found to be sandwiched between GO sheets, forming rough yet hierarchical structures. Clearly, these results revealed that the carbon sphere nanospacers effectively distanced GO sheets and prevented their close stacking. As the carbon sphere content increased, the thickness of the as-deposited GCHN film increased due to the larger amount of carbon spheres inserted among graphene sheets, thereby preventing the aggregation of GO sheets more efficiently (Fig. 2E). Moreover, the thickness of the GCHN material was dependent on the deposition time. Fig. 2F shows the relationship between the thickness of the GCHN material and the deposit time in the solution containing 50.0 wt% GO. In general, the thickness of the GCHN film increased quickly at the initial deposition process, and then slowed down during the course of deposition.

The mixed carbon-based coatings (*i.e.*, GCHN) were then employed as an active material to construct supercapacitor

electrodes and the corresponding fibrous and flexible supercapacitors (FFSCs). To investigate the synergy between carbon nanosphere fillers and the resulting capacitance properties of graphene/carbon sphere composites, electrochemical measurements were performed by varying the amount of GO under otherwise identical experimental conditions. Fig. 3A shows the CV curves of the FFSC electrodes with three different GO contents: pristine GO, 50.0 wt% and 33.3 wt%. All CV curves displayed a rectangular shape, indicating an efficient EDLC was established in the graphene-based electrodes, imparting good charge propagation within the electrodes. Under the identical electrode construction and experimental conditions, the CV curves of the two hierarchical nanostructured, mixed-carbon material electrodes (50.0 wt% and 33.3 wt% of GO content) had a larger encircled area than that of the pristine GO-based electrode. This implied that the electrochemical capacitance performance of the hierarchically structured electrodes (*i.e.*, GCHN) improved when the carbon nanospheres were added as nanospacers and increased the active area. Although an effective conductive network was formed by the rGO nanosheets, the ions cannot be freely accessed because of the small distance between the interlayers of graphene nanosheets. The rGO can pile up *via* π–π interactions with a smaller interlayer distance (~0.34 nm) for ion access.[17] As the content of carbon nanospheres increased, the amount of graphene surface area accessible to electrolyte ions was enhanced. However, the accessibility of this active area to electrolyte ions would decrease with excess carbon sphere content. This is no surprising as the excessive agglomerations of insulating carbon spheres would prevent graphene from forming a conductive network, thus deteriorating the charge storage capacity. At a scan rate of 80 mV s^{-1}, the specific capacity of the electrode with the 50.0 wt% GO content significantly improved, achieving a maximum value. As evidenced in the CV curves, this value was approximately 3 times greater than that of the electrode with pristine GO or 33.3 wt% GO content (Fig. 3B).

Electrical conduction and ion transfer were investigated by electrochemical impedance spectroscopy (EIS) in a frequency range of 0.1 Hz to 10 kHz (Fig. 3C). The inset showed the corresponding equivalent circuit model. The bulk resistance (R_s) for the pristine GO electrode was found to be 1.69 Ω, which is lower than the value of 2.07 Ω obtained from the electrode containing the 50.0 wt% GO. This can be ascribed to the presence of nonconductor carbon spheres between the GO layers to form hierarchical nanostructures. The R_{ct} of the 50.0 wt% GO electrode was also much higher than the pristine GO electrode (Fig. 3D) as the insertion of nonconductor carbon spheres decreased the exchange rate of the electrode and electrolyte ions. Furthermore, the slope of the plot at the low frequency of the 50.0 wt% GO electrode was higher than that of the pristine GO electrode, indicating the characteristics of a porous electrode strongly controlled by the diffusive resistivity of the electrolyte within the pores of the electrode material.[49–52] The hierarchical nanostructures with carbon spheres and graphene enhanced the ion diffusion in the electrode material. As a result, the diffusing line of the electrode displayed an ideal straight line along the imaginary axis as shown in Fig. 3C.

In order to gain more insight into electrochemical performance, CV analysis was performed on 50.0 wt% GO GCHN electrodes at various scan rates in the range of 10–160 mV s^{-1} (Fig. 3E). All CV curves of GCHN electrodes displayed nearly rectangular shapes at even very high scan rates, suggesting the formation of an efficient EDLC in the graphene-based electrodes. The shapes were also indicative of good charge propagation within the electrodes.[53] The GCD curves of electrodes with 50.0 wt% GO content were measured at different current densities from 0.8–6.4 mA cm^{-2}. All curves were linear and symmetric and close to a triangular shape, signifying the typical EDLC behavior. Clearly, the shapes of the electrodes demonstrated excellent electrochemical reversibility and charge/discharge properties (Fig. 3F).[54]

In the present study, the GCHN fiber electrode with the optimal 50.0 wt% GO content and 4.5 μm in thickness was further utilized as an active material to construct the supercapacitors (Fig. 4A). Fig. 4B compares the CV behaviors of FFSC devices measured at various scan rates. The nearly rectangular shapes even at very high scan rates up to 1000 mV s^{-1} indicated an efficient EDLC. However, when the scan rate was further increased to 2000 mV s^{-1}, the rectangle shape became severely distorted, converting into a diamond shape, indicating a poor capacitance performance.

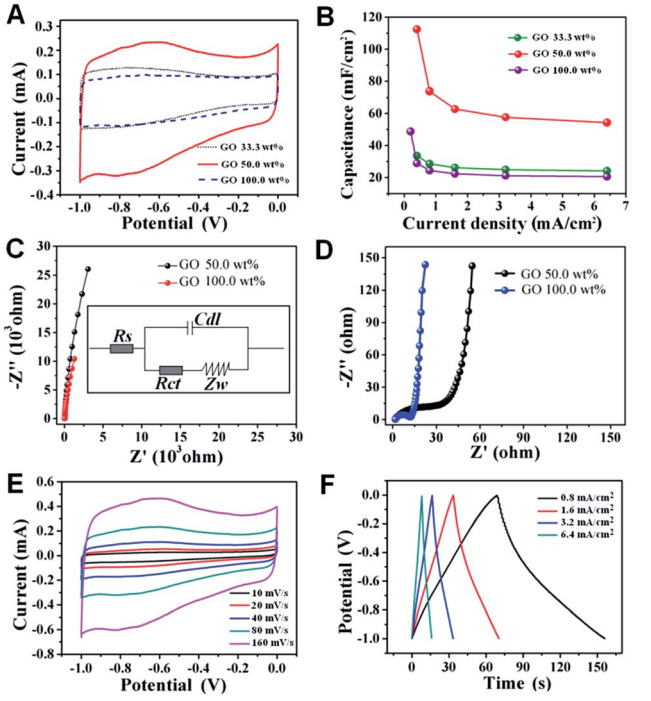

Fig. 3 (A) CV curves of electrodes with different GO contents: pristine GO, 50.0 wt%, and 33.3 wt%, at a scan rate of 80 mV s^{-1}. (B) The specific capacitances of electrodes based on pristine GO, 50.0 wt%, and 33.3 wt% GO content, from the CV curves at various scan rates. (C) Nyquist plot of the electrodes based on pristine GO and 50.0 wt%. The inset in (C) is the equivalent circuit. (D) is an enlarged view of (C). (E) CV curves of the GCHN electrode with 50.0 wt% GO content at various scan rates. (F) GCD curves of the GCHN electrode with GO content of 50.0 wt% at various discharge current densities.

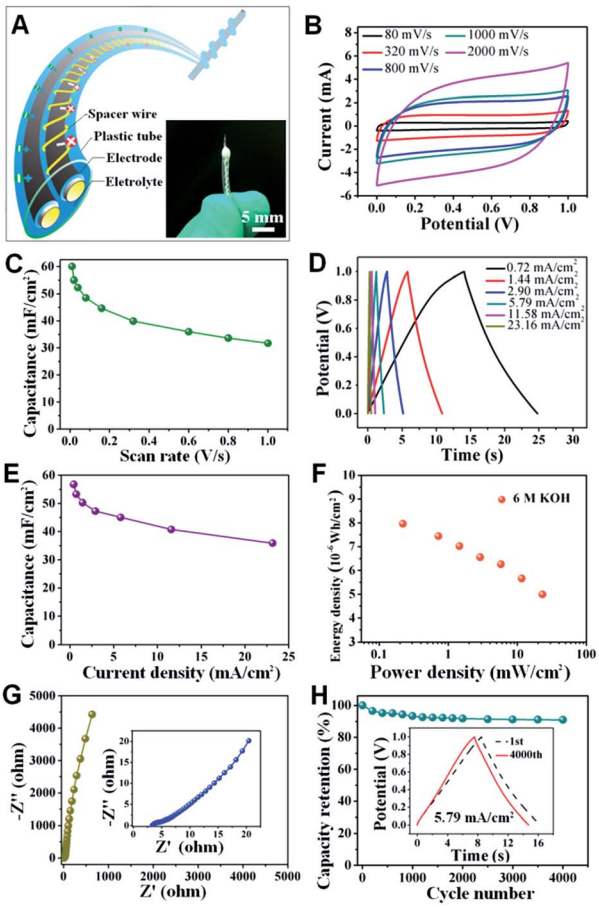

Fig. 4 Electrochemical characterization of the FFSC with an active electrode length of 11 mm and a diameter of 100 μm in a 6.0 mol L^{-1} KOH electrolyte. (A) Schematic diagram of the FFSC device with a special encapsulating technique and a digital image of the assembled FFSC device. (B) CV curves of the FFSC at various scan rates. (C) The specific capacitances from CV curves at various scan rates. (D) GCD curves of the FFSC with 50 wt% GO content at various discharge current densities. (E) The specific capacitances at various discharge current densities. (F) Ragone plot for the FFSC. (G) The Nyquist plot and its close-up view of the FFSC in a 6.0 mol L^{-1} KOH electrolyte. (H) The GCD curves of the 1st and 4000th cycles at a charge/discharge current density of 5.79 mA cm^{-2}.

The areal capacitance of the FFSC can be calculated based on CV curves, according to eqn (1):

$$C = \int \frac{I}{A} \mathrm{d}v \Big/ (k\Delta U) \quad (1)$$

where C is the areal capacitance (mF cm^{-2}), I is the response current (mA), A is the surface area of fiber electrodes, ΔU is the potential range of CV curves (V), k is the potential scan rate (mV s^{-1}), and I/A is the current density (mA cm^{-2}). The diameter of fiber was 100.0 μm, and the length of active material was 1.1 cm.

In general, an increase in the integrated area of the current–potential curve is associated with an increased scan rate, suggesting a good storage rate ability. However, a decrease in specific capacitance with increase in scan rate was observed as shown in Fig. 4C. The areal capacitance of the FFSC calculated

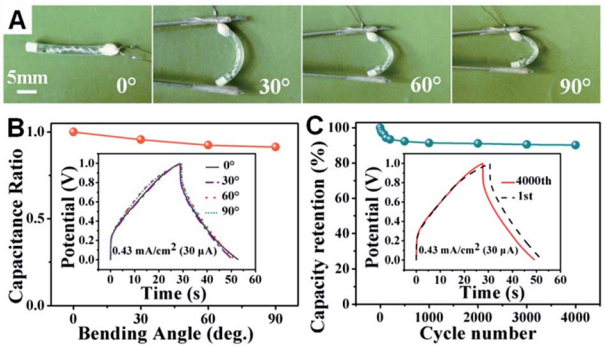

Fig. 5 The performance of the supercapacitor examined at different bending states. (A) Digital images of the supercapacitor bent at different angles. (B) Capacitance ratio for the supercapacitor at different angles and curves of the supercapacitor bent at different angles. (C) The GCD curves of the 1st and 4000th cycles at a charge/discharge current density of 0.43 mA m^{-2} of the SFSC after 10 bending times.

from the CV curve was from 60.02 mF cm^{-2} to 31.73 mF cm^{-2} when the scan rate increased from 10 mV s^{-1} to 1000 mV s^{-1}, respectively. At a scan rate of 1000 mV s^{-1}, the calculated capacitance of the FFSC device was still as high as 31.73 mF cm^{-2}, which is higher than the reported areal capacitance of a fibrous flexible supercapacitor-based pen ink (1.7 mF cm^{-2})[41] as well as micro-supercapacitor-based carbon-onion (9.5 mF cm^{-2}) under an identical scan rate.[19]

The areal capacitance of the FFSC can be calculated by dividing the electric quantity by the discharge time, according to eqn (2):

$$C = \frac{Q}{S\Delta V} = \frac{\int I \mathrm{d}t}{S\Delta V} = \frac{It_{\mathrm{discharge}}}{S\Delta V} = \frac{I}{2\pi DL} \times \frac{t_{\mathrm{discharge}}}{V - \mathrm{IR}_{\mathrm{drop}}} \quad (2)$$

where Q is the electric quantity during discharge, I is the constant applied current (mA), $t_{\mathrm{discharge}}$ is the discharge time (s), S is the surface area of fiber electrodes, D is the diameter of the electrode (cm), L is the hierarchical nanostructure compound materials on the platinum wire (1.1 cm), and ΔV is the potential range of discharge (V). $\mathrm{IR}_{\mathrm{drop}}$ is the voltage drop at the beginning of discharge, and this value was ignored as no obvious voltage drop occurred in the galvanostatic charge/discharge curves.

The galvanostatic charge/discharge behaviors of the FFSC at different current densities from 0.43 mA cm^{-2} to 23.16 mA cm^{-2} are shown in Fig. 4D. The symmetric and near linear slopes were observed even at the current density exceeding 20 mA cm^{-2}, indicating an efficient EDLC formation. Moreover, the voltage dropped at the beginning of the discharge curves, reflecting a relatively low equivalent series resistance. As the current density increased from 0.43 mA cm^{-2} to 23.16 mA cm^{-2}, there was a decrease in specific capacitance from 53.56 mF cm^{-2} to 35.90 mF cm^{-2} accordingly. This can be attributed to the difference in the insertion–desertion behavior of ions from the electrolyte to the electrode material. The OH^- ions failed to fully occupy the active sites at the electrolyte/electrode interface under higher current densities due to the limited ion

migration velocity and limited transporting routes at the interface, leading to an uncompleted insertion reaction. There was a drop of 33.0% from the initial capacitance as the current density increased from 0.43 mA cm^{-2} to 23.16 mA cm^{-2} (Fig. 4E).

The energy density and power density of the fibrous supercapacitor can be obtained based on the following equations:

$$E = \frac{1}{2}CV^2 \quad (3)$$

$$P = \frac{E}{t_{\text{discharge}}} \quad (4)$$

where E is the energy density (10^{-6} W h cm^{-2}), P is the power density (mW cm^{-2}) of the supercapacitor, C is the areal capacitance (mF cm^{-2}), and V is the operating voltage (V). The energy density of the FFSC decreased from 7.96×10^{-6} W h cm^{-2} to 4.99×10^{-6} W h cm^{-2}, while the power density increased from 0.22 mW cm^{-2} to 23.16 mW cm^{-2} when the current density increased from 0.43 mA cm^{-2} to 23.16 mA cm^{-2}, respectively (Fig. 4F). These results are comparable to the reported values (energy density: 10^{-6} to 10^{-4} W h cm^{-2}, power density: 10^{-3} to 10^{-1} W cm^{-2}) of carbon-based supercapacitors and metal oxide-based supercapacitors.[38,55–57] However, the power density and energy density could be further improved by incorporating more fibers in the device, scale-up process or coaxial assembly construction.

In order to scrutinize the properties of conductivity and charge transport of the supercapacitor, EIS measurements were also performed. In general, the Nyquist plot of the FFSC contains a semi-circle at high frequency and an inclined line at low frequency indicating an ideal capacitive behavior with excellent charge transfer and diffusion (Fig. 4G). In the high frequency region, the intercept of the curve with the real axis (Re(Z)) corresponded to the total resistance (ESR), resulting from the resistances from the electrolyte (R_s), electrodes (R_e) and the contact (R_c) between the electrode and the current collector. In the high frequency region, the ESR was 3.39 Ω at a frequency of 96.7 kHz. This was an important parameter in determining the charge/discharge rate and power density of a supercapacitor.[47] The ESR value also indicated the quality of graphene conductivity, as well as the efficiency of electrolyte ion access to the surface of the hierarchical nanostructure. In the mid-frequency to high-frequency range, the semicircle associated with the surface properties of the electrode corresponded to interfacial contact capacitance (C_c) and charge transfer resistance (R_{ch}). The charge-transfer resistance was found to be 4.8 Ω, which was in the same order of magnitude as other carbon materials due to the isolation of carbon nanospheres. Furthermore, the impedance curve intersected to the real axis (Re(Z)) was at 45°, which was consistent with the porous nature of the electrode when saturated with electrolytes,[58] signifying a good capacitive behavior. The more vertical the curve, the more closely the supercapacitor behaved as an ideal capacitor.[50] Interestingly, the maximum phase angle of the FFSC was −81.8°, which was close to an ideal capacitor's maximum phase angle of −90°.

The cycle stability of the FFSC device is a crucial parameter for practical applications. In order to further evaluate the electrochemical stability, the GCD cycling stability of hierarchically structured supercapacitors was examined over a large number of charge/discharge cycles at a current density of 5.79 mA cm^{-2} in a 6.0 M KOH electrolyte. As shown in Fig. 4H, the GCHN displayed an excellent long cycle lifetime. After 4000 charge/discharge cycles, the GCD curve still remained undistorted and essentially symmetric. The capacitance retained 91.2% of the initial capacitance after 4000 GCD cycles, and only decreased approximately 4% during 100 charge/discharge cycles, demonstrating an excellent cyclic stability of FFSC devices. The remarkable stability may be primarily due to the existence of a stable and unique 3D GCHN network that acted as a double-layer capacitor, as well as the synergy originating from the firm integration between carbon nanospheres and GO nanosheets.

For viable applications, it is required that the supercapacitor is leak-free, flexible, and safe.[59,60] To this end, an all-solid-state flexible supercapacitor (SFSC) was recently developed.[61] In this work, as a proof-of-concept, we successfully constructed SFSC devices by using a H_3PO_4–polyvinyl alcohol (PVA) gel electrolyte and investigated the effect of curvature on the SFSC performance was explored by exposing it to different bending states, as illustrated in Fig. 5A. It is worth noting that no obvious changes of charge and discharge time from the GCD curves of the device between 0 and 90° were observed, and the capacitance ratio remained steady (Fig. 5B), with only a slight drop under the high curvature for a 1.6 cm long SFSC, revealing that the electrochemical performance of the SFSC was stable under different bending angles. Moreover, the capacitance of the SFSC after 10 bending numbers still retained 90.1% of the initial capacitance after 4000 GCD cycles (Fig. 5C), indicating a good bending stability of the SFSC. We believe the bending stability of the SFSC can be further enhanced with optimized packing techniques. Clearly, crafting a robust GCHN by the synergy between carbon spheres and GO nanosheets opens new opportunities for designing and constructing high-performance electrochemical supercapacitor devices, and demonstrates promising applications in flexible energy devices.

Conclusions

In summary, hierarchical composites comprising GO nanosheets and carbon nanospheres with a unique layer-by-layer structure were crafted by a one-step electrochemical deposition method. The electrochemical performance and cyclic stability of the resulting GO nanosheets and carbon nanospheres hierarchical nanostructure (GCHN) composite materials on the fibrous Pt electrode under the different experimental conditions such as the mass ratio and deposition duration were explored and optimized. Compared to pristine GO nanosheet, the porous GCHN materials displayed a highly enhanced capacitance. Such a hierarchical carbon-based structure provides a versatile platform for many promising applications, including supercapacitors, lithium ion batteries, sensors, and other fiber-shaped devices. As a proof-of-concept, a fibrous and flexible supercapacitor with excellent electrochemical performance was

constructed and possessed an optimal capacitance of 53.56 mF cm^{-2} and a good reversible charge/discharge ability without a significant loss of capacitance (approximately 91.2% retained after 4000 cycles). Quite intriguingly, an all-solid-state flexible supercapacitor with stable electrochemical activity was successfully realized under various bending angles (up to 90°). We envision that this simple yet robust preparative strategy can be easily extended to construct a wide diversity of graphene-based fibrous and flexible composites with superior electrochemical performance for energy materials and devices.

Notes and references

1 F. Bonaccorso, L. Colombo, G. H. Yu, M. Stoller, V. Tozzini, A. C. Ferrari, R. S. Ruoff and V. Pellegrini, *Science*, 2015, **347**, 6217.
2 I. V. Lightcap and P. V. Kamat, *Acc. Chem. Res.*, 2013, **46**, 2235.
3 W. X. Guo, C. Xu, X. Wang, S. H. Wang, C. F. Pan, C. J. Lin and Z. L. Wang, *J. Am. Chem. Soc.*, 2012, **134**, 4437.
4 Y. X. Tang, Y. Y. Zhang, J. Y. Deng, J. Q. Wei, H. L. Tam, B. K. Chandran, Z. L. Dong, Z. Chen and X. D. Chen, *Adv. Mater.*, 2014, **26**, 6111.
5 C. C. Chen, L. T. Dou, R. Zhu, C. H. Chung, T. B. Song, Y. B. Zheng, S. Hawks, G. Li, P. S. Weiss and Y. Yang, *ACS Nano*, 2012, **6**, 7185.
6 G. H. Yu, L. B. Hu, M. Vosgueritchian, H. L. Wang, X. Xie, J. R. McDonough, X. Cui, Y. Cui and Z. N. Bao, *Nano Lett.*, 2011, **11**, 2905.
7 W. Chen, R. B. Rakhi, L. B. Hu, X. Xie, Y. Cui and H. N. Alshareef, *Nano Lett.*, 2011, **7**, 5165.
8 G. P. Wang, L. Zhang and J. J. Zhang, *Chem. Soc. Rev.*, 2012, **41**, 797.
9 Z. Q. Niu, L. L. Liu, L. Zhang, Q. Shao, W. Y. Zhou, X. D. Chen and S. S. Xie, *Adv. Mater.*, 2014, **26**, 3681.
10 J. S. Bonso, G. D. Kalaw and J. P. Ferraris, *J. Mater. Chem. A*, 2014, **2**, 418.
11 L. L. Zhang, Y. Gu and X. S. Zhao, *J. Mater. Chem. A*, 2013, **1**, 9395.
12 X. H. Li, G. Y. Wang, X. W. Wang, X. P. Li and J. H. Ji, *J. Mater. Chem. A*, 2013, **1**, 10103.
13 H. R. Byon, S. W. Lee, S. Chen, P. T. Hammond and Y. Shao-Horn, *Carbon*, 2011, **49**, 457.
14 K. S. Novoselov, A. K. Geim, S. V. Morozov, D. Jiang, M. I. Katsnelson, I. V. Grigorieva, S. V. Dubonos and A. A. Firsov, *Nature*, 2005, **438**, 197.
15 L. Wang, X. P. Lu, S. B. Lei and Y. H. Song, *J. Mater. Chem. A*, 2014, **2**, 4491.
16 H. L. Wang, L. F. Cui, Y. Yang, H. S. Casalongue, J. T. Robinson, Y. Y. Liang, Y. Cui and H. J. Dai, *J. Am. Chem. Soc.*, 2010, **132**, 13978.
17 M. D. Stoller, S. Park, Y. Zhu, J. An and R. S. Ruoff, *Nano Lett.*, 2008, **8**, 3498.
18 Q. Wu, Y. Xu, Z. Yao, A. Liu and G. Shi, *ACS Nano*, 2010, **4**, 1963.
19 D. W. Wang, F. Li, J. Zhao, W. Ren, Z. G. Chen, J. Tan, Z. S. Wu, I. Gentle, G. Q. Lu and H. M. Cheng, *ACS Nano*, 2009, **3**, 1745.
20 N. Mahmood, C. Z. Zhang, H. Yin and Y. L. Hou, *J. Mater. Chem. A*, 2014, **2**, 15.
21 K. W. Shu, C. Y. Wang, M. Wang, C. Zhao and G. G. Wallace, *J. Mater. Chem. A*, 2014, **2**, 1325.
22 A. M. Silva, M. S. Pires, V. N. Freire, E. L. Albuquerque, D. L. Azevedo and E. W. S. Caetano, *J. Phys. Chem. C*, 2010, **114**, 17472.
23 X. L. Wang, H. Bai, Z. Y. Yao, A. R. Liu and G. Q. Shi, *J. Mater. Chem.*, 2010, **20**, 9032.
24 A. H. Castro Neto, F. Guinea, N. M. R. Peres, K. S. Novoselov and A. K. Geim, *Rev. Mod. Phys.*, 2009, **81**, 109.
25 G. K. Dimitrakakis, E. Tylianakis and G. E. Froudakis, *Nano Lett.*, 2008, **8**, 3166.
26 S. P. Wu, R. Wang, Z. L. Wang and Z. Q. Lin, *Nanoscale*, 2014, **6**, 8350.
27 W. J. Zhou, X. H. Cao, Z. Y. Zeng, W. H. Shi, Y. Y. Zhu, Q. Y. Yan, H. Liu, J. Y. Wang and H. Zhang, *Energy Environ. Sci.*, 2013, **6**, 2216.
28 H. Wang, R. Kou, D. Choi, Z. G. Yang, Z. M. Nie, J. Li, L. V. Saraf, D. H. Hu, J. G. Zhang, G. L. Graff, J. Liu, M. A. Pope and I. A. Aksay, *ACS Nano*, 2010, **4**, 1587.
29 Z. Weng, Y. Su, D. W. Wang, F. Li, J. H. Du and H. M. Cheng, *Adv. Energy Mater.*, 2011, **1**, 917.
30 Y. Yang, Z. W. Peng, G. N. Wang, G. D. Ruan, X. J. Fan, L. Li, H. L. Fei, R. H. Hauge and J. M. Tour, *ACS Nano*, 2014, **8**, 7279.
31 Y. Yang, H. L. Fei, G. D. Ruan, C. S. Xiang and J. M. Tour, *Adv. Mater.*, 2014, **26**, 8163.
32 T. Kim, G. Jung, S. Yoo, S. S. Kwang and R. S. Ruoff, *Adv. Energy Mater.*, 2013, **7**, 6899.
33 C. H. Xu, B. H. Xu, Y. Gu, Z. G. Xiong, J. Sun and X. S. Zhao, *Energy Environ. Sci.*, 2013, **6**, 1388.
34 A. V. Murugan, T. Muraliganth and A. Manthiram, *Chem. Mater.*, 2009, **21**, 5004.
35 J. X. Zhu, D. Yang, Z. Y. Yin, Q. Y. Yan and H. Zhang, *Small*, 2014, **10**, 3480.
36 J. Ren, L. Li, C. Chen, X. Chen, Z. Cai, L. Qiu, Y. Wang, X. Zhu and H. Peng, *Adv. Mater.*, 2013, **25**, 1155.
37 Z. Cai, L. Li, J. Ren, L. Qiu, H. Lin and H. Peng, *J. Mater. Chem. A*, 2013, **1**, 258.
38 Y. P. Fu, X. Cai, H. W. Wu, Z. B. Lv, S. C. Hou, M. Peng, X. Yu and D. C. Zou, *Adv. Mater.*, 2012, **24**, 5713.
39 C. Z. Meng, C. H. Liu, L. Z. Chen, C. H. Hu and S. S. Fan, *Nano Lett.*, 2010, **10**, 4025.
40 S. Y. Wang and R. A. W. Dryfe, *J. Mater. Chem. A*, 2013, **1**, 5279.
41 C. X. Guo and C. M. Li, *Energy Environ. Sci.*, 2011, **4**, 4504.
42 Q. F. Wang, X. F. Wang, J. X. Ouyang, X. J. Hou, D. Chen, R. M. Wang and G. Z. Shen, *Nano Energy*, 2014, **8**, 44.
43 P. H. Yang and W. J. Mai, *Nano Energy*, 2014, **8**, 274.
44 T. Sakaki, M. Shibata, T. Miki, H. Hirosue and N. Hayashi, *Bioresour. Technol.*, 1996, **58**, 197.
45 C. X. Guo and C. M. Li, *Phys. Chem. Chem. Phys.*, 2010, **12**, 12153.
46 X. M. Sun and Y. D. Li, *Angew. Chem., Int. Ed.*, 2004, **43**, 597.
47 W. S. Hummers and R. E. Offeman, *J. Am. Chem. Soc.*, 1958, **80**, 1339.

48 Y. Wang, Z. Q. Shi, Y. Huang, Y. F. Ma, C. Y. Wang, M. M. Chen and Y. S. Chen, *J. Phys. Chem. C*, 2009, **113**, 13103.
49 Z. He and F. Mansfeld, *Energy Environ. Sci.*, 2009, **2**, 215.
50 S. S. Zhang, K. Xu and T. R. Jow, *Electrochim. Acta*, 2004, **49**, 1057.
51 S. J. Bao, Y. Y. Liang, W. J. Zhou, B. L. He and H. L. Li, *J. Power Sources*, 2006, **154**, 239.
52 C. Lin, J. A. Ritter and B. N. Popov, *J. Electrochem. Soc.*, 1998, **145**, 4097.
53 J. F. Zang, S. J. Bao, C. M. Li, H. J. Bian, X. Q. Cui, Q. L. Bao, C. Q. Sun, J. Guo and K. R. Lian, *J. Phys. Chem. C*, 2008, **112**, 14843.
54 J. Yan, T. Wei, B. Shao, F. Q. Ma, Z. J. Fan, M. L. Zhang, C. Zheng, Y. C. Shang, W. Z. Qian and F. Wei, *Carbon*, 2010, **48**, 1731.
55 V. T. Le, H. Kim, A. Ghosh, J. Kim, J. Chang, Q. A. Vu, D. T. Pham, J. Lee, S. Kim and Y. H. Lee, *ACS Nano*, 2013, **7**, 5940.
56 J. H. Kim, S. H. Kang, K. Zhu, J. Y. Kim, N. R. Neale and A. J. Frank, *Chem. Commun.*, 2011, **47**, 5214.
57 J. Bae, M. K. Song, Y. J. Park, J. M. Kim, M. L. Liu and Z. L. Wang, *Angew. Chem., Int. Ed.*, 2011, **50**, 1683.
58 C. M. Niu, E. K. Sichel, R. Hoch, D. Moy and H. Tennent, *Appl. Phys. Lett.*, 1997, **70**, 1480.
59 Q. F. Wang, X. F. Wang, B. Liu, G. Yu, X. J. Hou, D. Chen and G. Z. Shen, *J. Mater. Chem. A*, 2013, **1**, 2468.
60 X. D. Zhang, Z. Y. Lin, B. Chen, S. Sharma, C. P. Wong, W. Zhang and Y. L. Deng, *J. Mater. Chem. A*, 2013, **1**, 5835.
61 L. Y. Yuan, X. Xiao, T. P. Ding, J. W. Zhong, X. H. Zhang, Y. Shen, B. Hu, Y. H. Huang, J. Zhou and Z. L. Wang, *Angew. Chem., Int. Ed.*, 2012, **51**, 4934.

